THE JOURNAL OF PHYSICAL CHEMISTRY Letters

Letter

pubs.acs.org/JPCL

Two-Photon Absorption Spectrum of a Single Crystal Cyanine-like Dye

Honghua Hu,[†] Dmitry A. Fishman,[†] Andrey O. Gerasov,[‡] Olga V. Przhonska,[†,§] Scott Webster,[†] Lazaro A. Padilha,[∥] Davorin Peceli,[†] Mykola Shandura,[‡] Yuriy P. Kovtun,[‡] Alexey D. Kachkovski,[‡] Iffat H. Nayyar,[⊥,#,▽,○] Artëm E. Masunov,[⊥,#,▽,○] Paul Tongwa,[◆] Tatiana V. Timofeeva,[◆] David J. Hagan,[†,▽] and Eric W. Van Stryland*[,†,▽]

[†]CREOL, The College of Optics and Photonics, University of Central Florida, Orlando, Florida 32816, United States

[‡]Institute of Organic Chemistry, National Academy of Sciences, Murmanskaya 5, Kiev, 03094, Ukraine

[§]Institute of Physics, National Academy of Sciences, Prospect Nauki 46, Kiev, 03028, Ukraine

[∥]Center for Advanced Solar Photophysics, Los Alamos National Laboratory, Los Alamos, New Mexico 87545, United States

[⊥]NanoScience Technology Center, University of Central Florida, Orlando, Florida 32826, United States

[#]Department of Chemistry, University of Central Florida, Orlando, Florida 32816, United States

[▽]Department of Physics, University of Central Florida, Orlando, Florida 32816, United States

[○]Florida Solar Energy Center, University of Central Florida, Orlando, Florida 32816, United States

[◆]Department of Biology and Chemistry, New Mexico Highlands University, Las Vegas, New Mexico 87701, United States

Supporting Information

ABSTRACT: The two-photon absorption (2PA) spectrum of an organic single crystal is reported. The crystal is grown by self-nucleation of a subsaturated hot solution of acetonitrile, and is composed of an asymmetrical donor-π-acceptor cyanine-like dye molecule. To our knowledge, this is the first report of the 2PA spectrum of single crystals made from a cyanine-like dye. The linear and nonlinear properties of the single crystalline material are investigated and compared with the molecular properties of a toluene solution of its monomeric form. The maximum polarization-dependent 2PA coefficient of the single crystal is 52 ± 9 cm/GW, which is more than twice as large as that for the inorganic semiconductor CdTe with a similar absorption edge. The optical properties, linear and nonlinear, are strongly dependent upon incident polarization due to anisotropic molecular packing. X-ray diffraction analysis shows π-stacking dimers formation in the crystal, similar to H-aggregates. Quantum chemical calculations demonstrate that this dimerization leads to the splitting of the energy bands and the appearance of new red-shifted 2PA bands when compared to the solution of monomers. This trend is opposite to the blue shift in the linear absorption spectra upon H-aggregation.

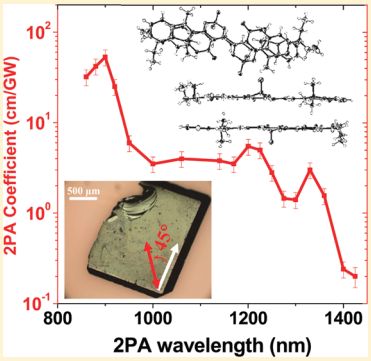

SECTION: Molecular Structure, Quantum Chemistry, and General Theory

Two-photon absorption (2PA), an instantaneous $\chi^{(3)}$ optical nonlinear process, has potential applications in microfabrication,[1,2] optical data storage,[3] optical limiting,[4] microscopic imaging,[5] and upconverted emission for laser applications.[6−8] The search for large 2PA materials spans from bulk solid-state materials (e.g., semiconductors[9]), to engineered nanostructured materials (e.g., semiconductor quantum dots[10]), and to organic molecules.[11,12] Organic molecules possess the advantage of greater degrees of freedom in custom material design and fabrication. With the capability to enhance nonlinear optical properties by directional modification of their molecular structures, cyanine-like dyes exhibit a linear extended π-conjugated system with π-electrons delocalized along the molecular backbone. They often manifest very large (up to 20 D[13]) transition dipole moments that can induce strong optical nonlinearities at the molecular level. Substitution with different end groups, i.e., electron donors (D) or electron acceptors (A), yields different structural architectures: symmetrical quadrupolar D-π-D[14] (or D-π-A-π-D), A-π-A[13] (or A-π-D-π-A), or asymmetrical dipolar D-π-A[15] (or push−pull) dyes demonstrating different optical properties. Significant effort is presently devoted to understanding the structure−property relations of these compounds to enhance molecular nonlinearities.[16] 2PA cross sections, as large as 33 000 GM, have been obtained for extended bis(donor) squaraines.[17] However, these measurements have been conducted mainly in

Received: February 27, 2012
Accepted: April 19, 2012
Published: April 19, 2012

isotropic solutions with relatively small concentration ($<10^{-3}$ M) in order to measure the intrinsic 2PA without introducing complications from various types of aggregation. In spite of significant progress in determining the main criteria for a predictive capability for nonlinear molecular properties,[16] there are still many remaining questions concerning what happens in the solid crystalline materials arising from strong molecular interactions. Despite the difficulties in growing single organic crystals of the size and optical quality required for nonlinear characterization, there are quite a few reports on the 2PA properties of organic materials in the solid phase.[18−22] One of very few examples showing a 2PA spectrum of single crystals of a conjugated polymer is poly[bis(*p*-toluene sulfonate) of 2,4-hexadiyne-1,6-diol] or PTS,[18] where the extremely large 2PA coefficient (up to 700 cm/GW) originates from the long π-conjugation chain, making it essentially a molecular quantum wire. Another report studied the two-photon excited emission properties of a single crystal made of cyano-substituted oligo(*p*-phenylenevinylene),[19] which shows strong anisotropy of the single crystal due to directional molecular packing. Similar polarization-dependent anisotropy in two-photon excited fluorescence and second-harmonic generation is also observed for single organic nanocrystals, which show enhanced optical nonlinearities.[20−22] However, no direct measurement of the 2PA spectrum of a single crystal cyanine-dye has been reported.

Here we report the degenerate 2PA (D-2PA) and non-degenerate 2PA (ND-2PA) spectrum, both linear and nonlinear anisotropy, X-ray diffraction analysis, and quantum chemical calculations of an organic single crystal composed of an asymmetrical cyanine-like D-π-A molecule. In this work, we utilize a simple solute precipitation technique in a hot subsaturated monomeric solution to promote crystal formation. Unlike the polymeric crystal growth described in ref 18, no polymerization is involved before, during, or after the growth process, which has been shown to result in inhomogeneous and multidomains of the crystal requiring further processing, such as annealing.[18] Such crystal growth processes without polymerization allow for a valid comparison between the single crystal form and the monomeric form in solution to identify the differences in the nonlinear spectroscopic properties. To the best of our knowledge, this is the first report of the 2PA spectrum of single crystals made from a cyanine-like dye.

The molecular structure of the D-π-A dye is shown in Figure 1a. The chemical name is 8-(diethylamino)-2,2-difluoro-5-oxo-(5H)-4-[3-(1,3,3-trimethylindolin-2-ylidene)-1-propenyl]-chromeno[4,3-d]-1,3,2-(2H)-dioxaborine, labeled as G19. The linear and nonlinear optical properties of this dye in solutions of different polarity, including a study of a series of these dyes having different conjugation lengths with identical end groups, has been reported by us previously.[15] A description of the crystal growth technique is presented in the Experimental Section. Figure 1b,c exhibits optical micrographs of a single crystal showing the lateral dimensions of 1.5 × 1 mm^2 and a thickness of ~370 μm. These images show the sharp facets and parallel surfaces suitable for optical measurements. The upper left corner of the crystal (Figure 1b) was damaged during mounting the sample before the measurements. The linear absorption spectrum of the solution form of G19 is shown in panel d and is composed of an intense cyanine-like band attributed to the $S_0 \rightarrow S_1$ transition, and weak linear absorption in the visible and UV region corresponding to absorption to higher excited states, $S_0 \rightarrow S_n$. The $S_0 \rightarrow S_1$ absorption peak is located at 2.17 eV (572 nm) and has a large extinction

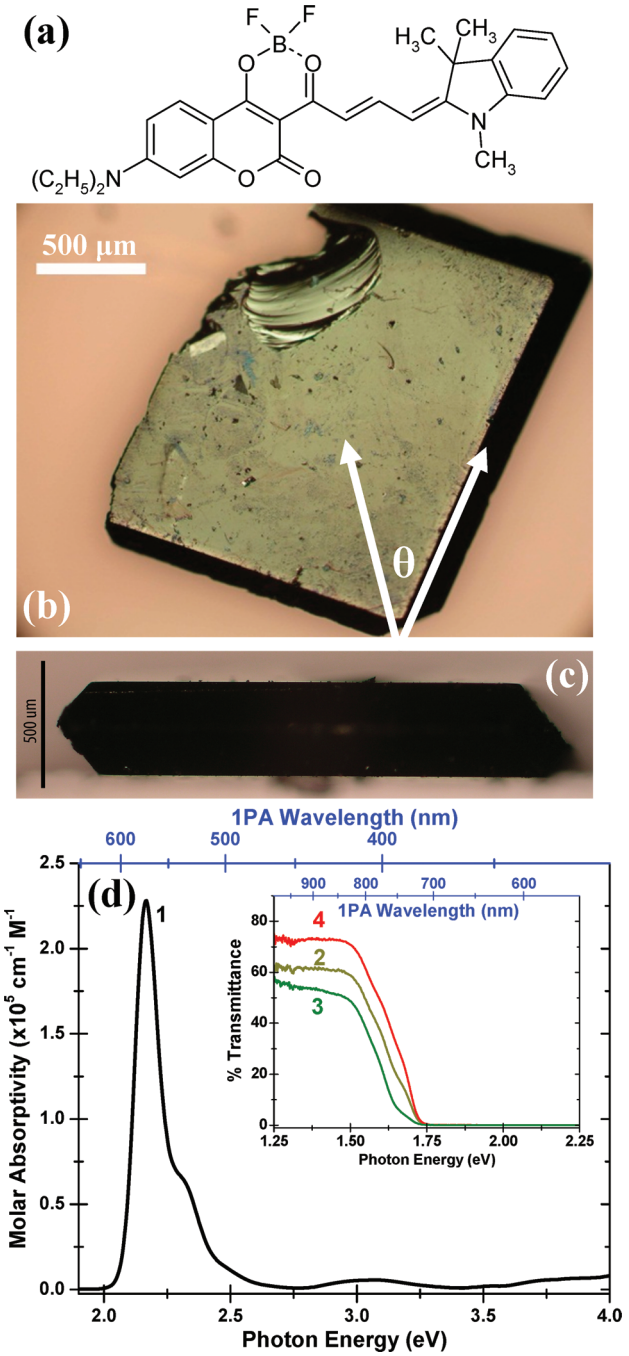

Figure 1. (a) Molecular structure of asymmetrical cyanine-like D-π-A molecule G19; (b) microscopic image of a G19 single crystal; (c) photograph of facet of the single crystal; (d) molar absorptivity of G19 in toluene (1) measured at ~10^{-6} M using a 1 cm cell, and linear transmittance of this G19 crystal using unpolarized light (2, inset), and with light polarized at θ = 45° (3), corresponding to a calculated refractive index of 3.2 and 2.3 at θ = 135° (4), both based on Fresnel reflections.

coefficient in toluene of 2.28 × 10^5 M^{-1} cm^{-1} (transition dipole moment of ~12.6 D[15]). The linear transmittance spectrum of the single crystal using unpolarized light is shown in the inset of Figure 1d. The one-photon absorption (1PA) edge is ~1.55 eV (800 nm). We also measured the linear transmittance spectra of this single crystal using polarized light with the polarization angle θ indicated in Figure 1b. We observed a large variation of transmittance and a slight shift of the 1PA edge with θ.

dx.doi.org/10.1021/jz300222h | J. Phys. Chem. Lett. 2012, 3, 1222−1228

Between 1.38 and 1.46 eV (850−900 nm) where the single crystal has a relatively small absorption, the lowest transmittance (~50%) is observed at θ = 45°, whereas the highest transmittance (~70%) is at θ = 135°. We assume that the variation of transmittance within the transparency range (<1.46 eV, or >850 nm) is mainly due to a polarization angle dependent refractive index leading to different reflection loss on both front and rear (100) surfaces of the single crystal; however, since there are inhomogeneities on the crystal surface, we cannot exclude the possibility that slight displacement of the probing spot position caused by rotation of a calcite polarizer may also induce transmittance change. Assuming no scattering loss, the reflection loss on each surface is ~21% determined by unpolarized light at 1.30 eV (950 nm) at normal incidence. By applying the Fresnel reflection law, we can estimate the averaged refractive index of the crystal to be ~2.7. The linear absorption peak for the crystal cannot be resolved due to the extremely large absorption coefficient and sample thickness. We also measured the reflection spectra of the single crystal with incident light polarized at θ = 45°, 90°, and 135° using reflection microscopy, as shown in Figure S1. The reflectivity at θ = 45° shows a large difference compared to θ = 135°. Also, only at θ = 45° and 135° is the polarization of the reflected light maintained. This indicates the alignment of the optic axis. The sinusoidal variation of reflectivity with respect to θ is shown in the inset of Figure S1 in the Supporting Information. Additionally, reflection microscopy and microellipsometery were unsuccessful in determining the peak linear absorption and refractive index of the single crystal due to its small size and probable complex reflection spectrum possibly containing real and imaginary parts of the linear permittivity.

To demonstrate the strong anisotropy of the spectroscopic characteristics of single crystal, we measured the polarization-dependent ND-2PA by a femtosecond copolarized excite-probe technique with an excitation and probe photon energy of 1.46 eV (corresponding to an excitation wavelength of 850 nm) and 1.30 eV (probe at 950 nm), respectively. Both the excitation and probe photon energies are below the linear absorption edge of the crystal. The corresponding ND-2PA coefficient, α_2^{ND}, is calculated from $dI_p/dz = -2\alpha_2^{ND} I_{ex} I_p$, where, I_{ex} and I_p are the irradiances of the excitation and probe beams, respectively. We record the linear transmittance (T_L) of the probe beam in the absence of excitation, and compare it with the nonlinear transmittance change (defined as $(T_L - T_{NL})/T_L$) of the probe beam as a function of its polarization angle θ (see Figure 1b) at zero temporal delay. Since the polarization angle is adjusted by rotating the half-wave plate placed in front of the crystal, no translation of the probe and pump beam is induced. Figure 2 shows the angular dependence of the linear transmittance and nonlinear transmittance change of the single crystal at probe photon energy 1.30 eV (950 nm), ~0.25 eV below the absorption edge. The linear transmittance reaches a minimum at ~45°, and a maximum at ~135° with respect to the long crystal growth facet as shown in Figure 1b. Since the linear absorption at the probe wavelength 950 nm is small (the losses of linear transmittance are due to Fresnel reflection and scattering), the minimum of the linear transmittance at $\theta \approx 45°$ suggests the largest refractive index, i.e., the largest linear polarizability of the crystal. The maximum nonlinear transmittance change is observed at θ = 45 ± 5°, and corresponds to α_2^{ND} = 50 ± 8 cm/GW, while the minimum, corresponding to α_2^{ND} = 14 ± 1.6 cm/GW, is observed at θ = 135 ± 5°. This observation is similar to the polarization angle dependent two-photon excited fluorescence of the single crystal made of cyano-substituted oligo(*p*-phenylenevinylene) discussed in ref 23, of which the fluorescence intensity is proportional to the 2PA coefficient at the corresponding polarization angle. Although the linear and nonlinear transmittance may vary with different spot positions on the sample due to surface defects, the coincidence of the angle for maximum nonlinear transmittance change with the angle for minimum linear transmittance of the probe beam reconfirms the orientation of the optic axis of the G19 crystal along the $\theta \approx 45°$ direction, which is also the direction of largest optical nonlinearity. The ND-2PA excite-probe data are shown in Figure S2(a) in the Supporting Information. By changing the probe wavelength, but keeping the excite photon energy fixed at 1.46 eV (850 nm), we also measured the ND-2PA spectrum at θ = 45° shown in Figure 3.

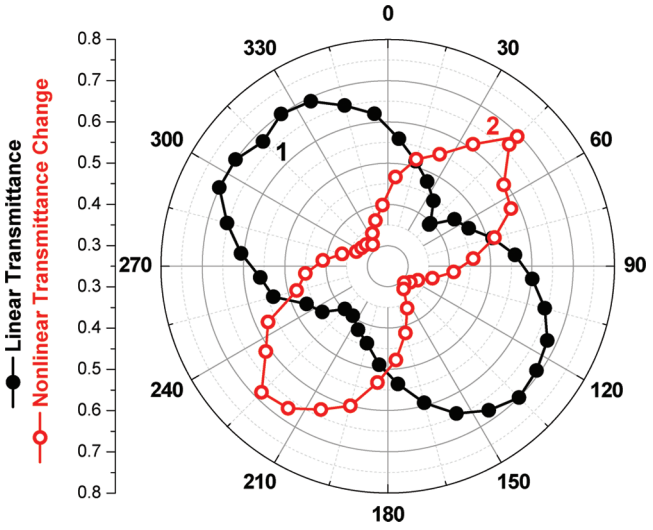

Figure 2. Linear transmittance (1) and nonlinear transmittance change at zero delay (2) of the G19 single crystal with respect to the polarization angle of the incident light. The scale is magnified so that the transmittance begins at the center with 0.25 and the outer ring is 0.8.

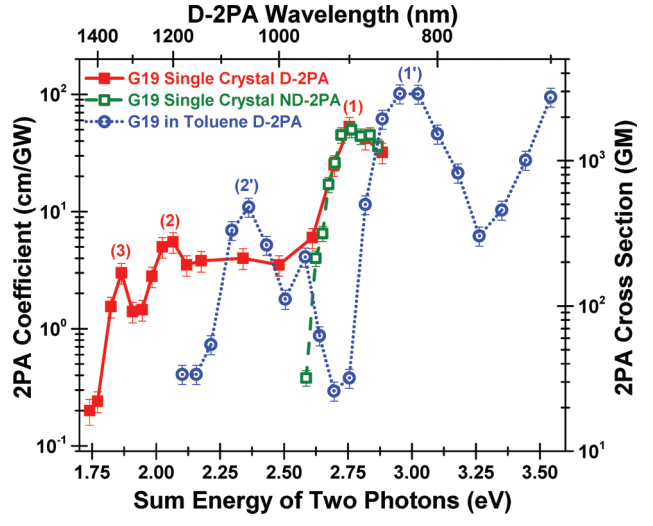

Figure 3. Comparison of D-2PA (red solid squares) and ND-2PA (green open squares) spectrum of G19 single crystal and its toluene solution (blue open circles) measured at a concentration of 8×10^{-5} M.

dx.doi.org/10.1021/jz300222h | *J. Phys. Chem. Lett.* 2012, 3, 1222−1228

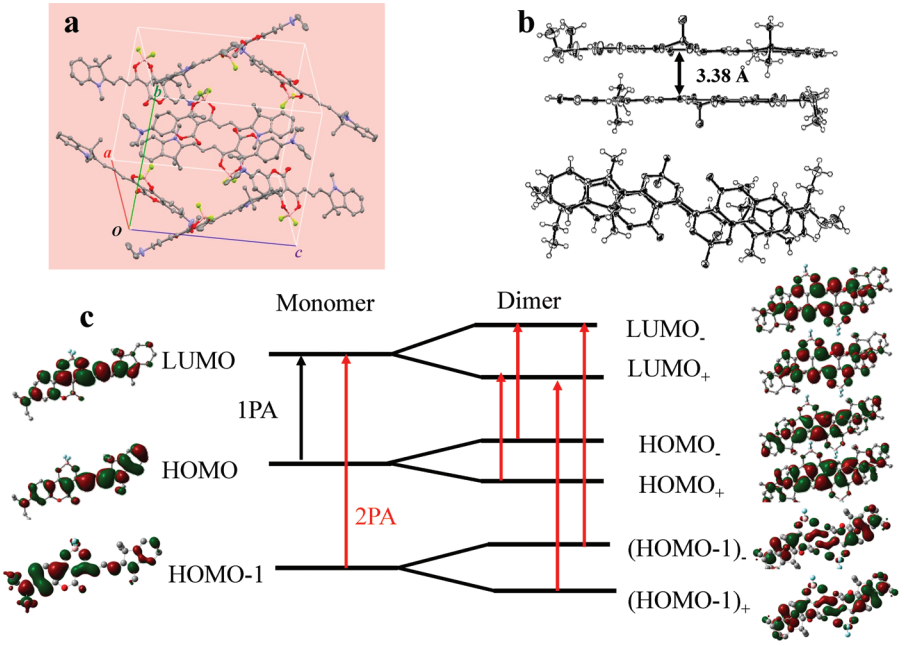

Figure 4. (a) Molecular packing in G19 single crystal; (b) formation of molecular π-stacking dimers aligned in an antiparallel mode; (c) schematic of formation of molecular orbitals in dimer from the molecular orbitals in monomer. The red and black arrows in the monomer illustrate 1PA and 2PA transitions, respectively. The red arrows in dimer illustrate the 2PA transitions (see explanation in the text).

A 2PA band is resolved with a peak transition at ~2.76 eV (excitation at 900 nm), which will be discussed in detail with the following experiments.

The D-2PA spectrum of the G19 single crystal is measured by open-aperture Z-scan with femtosecond pulses over the photon energy range from 0.87 to 1.44 eV (860−1425 nm), corresponding to two-photon transitions between 1.74 and 2.88 eV. The beam is polarized at $\theta = 45 \pm 5°$ to the crystal edge (as indicated in Figure 1b), at which angle the 2PA is maximized and the polarization state of the transmitted light is observed to be linear for all wavelengths studied. Figure 3 shows the resulting 2PA spectrum. We observe the strongest 2PA band from 2.61 to 2.88 eV (excitation from 860 to 950 nm) (marked as (1) in Figure 3) with a peak D-2PA coefficient (α_2) of 52 ± 9 cm/GW at the summed photon energy of 2.76 eV (corresponding to a D-2PA excitation at 900 nm). The D-2PA spectral shape over this wavelength range is consistent with the ND-2PA spectrum measured by the excite-probe technique. The Z-scan data at 2.76 eV (excitation at 900 nm) is shown in Figure S1(b) in the Supporting Information. It is well-known that the D-2PA coefficient of semiconductors can be *universally* scaled with E_g^{-3}, where E_g is the bandgap of the solid.[24] Therefore, to demonstrate the strong nonlinearity of the organic single crystal we compare the G19 single crystal, with an absorption edge of 1.55 eV (800 nm), to CdTe with a bandgap of 1.44 eV (861 nm).[25] The D-2PA coefficient is ~2.5× larger than the bulk semiconductor CdTe ($\alpha_2 = 21 \pm 3$ cm/GW at an excitation of 900 nm).[24] The largest 2PA band for the crystal is red-shifted by ~0.25 eV (~70 nm) compared to that of the corresponding toluene solution (also shown in Figure 3). By estimating the number density of molecules of the G19 crystal, determined by X-ray analysis (see unit cell deduced in Figure 4a), the average D-2PA cross section of an individual molecule in the single crystal at 2.76 eV is ~690 GM, which is approximately 4× smaller than the 2PA peak in the solution. Given that the 2PA cross section in isotropic solution is averaged by a factor of 5 due to the random orientation of solute molecules,[26] the reduction of the 2PA cross section in the crystal is ~20×. This is presumably due to strong molecular interactions between the closely spaced molecules in the crystal, as well as the different orientations of molecules inside the crystal unit cell (see Figure 4a). The positions of the next two lower energy 2PA bands (see Figure 3, labeled (2) and (3)) in the crystal are located at ~2.05 eV (excitation at ~1210 nm) and ~1.86 eV (excitation at ~1330 nm) with a peak α_2 of 5.5 ± 1.5 cm/GW and 3 ± 0.6 cm/GW, respectively. Figure 3 compares the spectral positions of the 2PA bands in the monomeric form to that of the single crystal. Note that we measure a 2PA cross section for the solution and a bulk 2PA coefficient for the crystal, so direct comparison of the 2PA magnitudes is avoided here due to the complex relative molecular orientation pattern in crystal (see Figure 4a). The D-2PA spectrum of the monomeric form in toluene, a low polarity solvent, exhibits three 2PA bands, as shown in Figure 3: (1) the first 2PA band between 2.75 - 3.31 eV (labeled as (1′) in Figure 3) with peak cross-section of ~3000 GM corresponding to a 2PA-allowed transition into the S_2 state; (2) a smaller 2PA band is observed between 2.25 - 2.61 eV (labeled as (2′) in Figure 3) with a peak cross-section of ~500 GM that is due to the vibrational coupling between S_1 and its vibrational mode; and (3) the strongest 2PA band related with a 2PA-allowed transition into higher-lying excited states (>3.5 eV), which cannot be fully resolved due to the onset of the 1PA edge. The origins of these 2PA bands in toluene is described in more detail in our previous paper.[15]

To help explain the origin of the 2PA bands in the single crystal, we analyze the structure with X-ray diffraction analyses at ~100 K. The crystal is orthorhombic, with space group *Pbca*, and unit cell parameters a = 15.861(2), b = 16.382(2), and c = 18.465(2) Å (Figure 4a). Crystallographic evaluation of the G19 morphology revealed that the most developed face of the crystal (shown in Figure 1b) corresponds to (100), i.e.,

dx.doi.org/10.1021/jz300222h | J. Phys. Chem. Lett. 2012, 3, 1222−1228

perpendicular to crystallographic axis oa shown in Figure 4a. By counting the number of molecules in the unit cell and calculating the volume of the unit cell, we estimate the number density of molecules of the crystal is $\sim 1.7 \times 10^{21}$ cm^{-3} (2.8 Mol L^{-1}). All the molecules in the crystal are symmetrically equivalent. They form centrosymmetric π-stacking dimers (one is shown in Figure 4a) with a separation between the molecular planes of ~3.38 Å. It has been shown that intermolecular interactions can alter the spectral properties significantly,[27,28] and that the crystalline environment, in turn, may enhance the intermolecular interactions.[29,30] In order to understand the optical properties of the crystal, we perform quantum chemical calculations using the standard TD-B3LYP/6-31G** method as implemented in the Gaussian 2003 suite of programs.[31] Our calculations indicate strong electronic coupling (c.a. 0.32 eV) between the molecules in one dimer (Figure 4c). Each unit cell in the crystal contains four such dimers in different orientations. Our calculations also show that the electronic coupling between the molecules in the adjacent dimers are only 3% compare to that inside the dimer (c.a. 0.01 eV). Therefore, the optical properties of the crystal are expected to be similar to the properties of the molecular dimers, slightly perturbed by the crystalline environment. In order to predict the absorption anisotropy, the angular dependence of the absorption by the molecular dimer needs to be averaged over the four specific orientations observed in the unit cell. However, this extends beyond the scope of the present work.

Quantum chemical calculations also reveal a different origin of 2PA in the solid state as compared to its monomeric form in solution. Results are shown schematically in Figure 4c and presented in Table 1. In the monomeric form, the main linear absorption peak is dominated by the highest occupied molecular orbital to lowest unoccupied molecular orbital (HOMO→LUMO) transition, and the strongest 2PA band (labeled (1′) in Figure 3) corresponds to the HOMO-1→LUMO transition. Dimerization around the center of symmetry (C_i) leads to a splitting of each electronic energy level into two: in-phase and out-of-phase linear combinations with opposite parities ($HOMO_+$ and HOMO_; $LUMO_+$ and LUMO_; etc.) as shown in Figure 4c.

Table 1. TD-B3LYP/6-31G Calculations for Transitions of the Monomer G19 and Corresponding Dimers**

transitions	oscillator strengths	final state symmetry	main configurations weighing factors | involved MOs
Monomer G19			
$S_0 \rightarrow S_1$	1.76	B_u	0.69|HOMO→LUMO>
$S_0 \rightarrow S_2$	0.04	A_g	0.68|HOMO-1→LUMO>
Dimer G19 Transitions Generated by $S_0 \rightarrow S_1$ Transitions of Monomer Molecules			
$S_0 \rightarrow S_1$	0	A_{g-}	0.60|$HOMO_+ \rightarrow LUMO_+$>−0.36| HOMO_→LUMO_>
$S_0 \rightarrow S_2$	0.07	B_{u-}	0.44|$HOMO_+ \rightarrow LUMO_-$>−0.56| HOMO_→$LUMO_+$>
$S_0 \rightarrow S_3$	0	A_{g+}	0.35|$HOMO_+ \rightarrow LUMO_+$>+0.60| HOMO_→LUMO_>
$S_0 \rightarrow S_4$	3.08	B_{u+}	0.53|$HOMO_+ \rightarrow LUMO_-$>+0.41| HOMO_→$LUMO_+$>
Dimer G19 Transitions Generated by $S_0 \rightarrow S_2$ Transitions of Monomer Molecules			
$S_0 \rightarrow S_5$	0.09	B_{u-}	0.32|$(HOMO\text{-}1)_+ \rightarrow LUMO_-$>−0.60| $(HOMO\text{-}1)_- \rightarrow LUMO_+$>
$S_0 \rightarrow S_6$	0	A_{g-}	0.53|$(HOMO\text{-}1)_+ \rightarrow LUMO_+$>−0.46| $(HOMO\text{-}1)_- \rightarrow LUMO_-$>
$S_0 \rightarrow S_7$	0.2	B_{u+}	0.61|$(HOMO\text{-}1)_+ \rightarrow LUMO_-$>+0.29| $(HOMO\text{-}1)_- \rightarrow LUMO_+$>
$S_0 \rightarrow S_8$	0	A_{g+}	0.43|$(HOMO\text{-}1)_+ \rightarrow LUMO_+$>+0.29| $(HOMO\text{-}1)_- \rightarrow LUMO_-$>

As a result, all electronic transitions in the dimer become mixed and split (mixed meaning "+" and "−" combinations, and split referring to an energy separation between these two combinations). According to our calculations (see Table 1), there are four transitions in the dimer generated by 1PA transitions $S_0 \rightarrow S_1$ in each monomer: two allowed $A_g \rightarrow B_u$ (with different oscillator strengths) and two forbidden $A_g \rightarrow A_g$ transitions with zero oscillator strength. Both allowed transitions $A_g \rightarrow B_u$ are formed by "+" and "−" combinations of $HOMO_+ \rightarrow LUMO_-$ and $HOMO_- \rightarrow LUMO_+$ transitions. Both forbidden transitions $A_g \rightarrow A_g$ are formed by "+" and "−" combinations of $HOMO_+ \rightarrow LUMO_+$ and $HOMO_- \rightarrow LUMO_-$ transitions. These transitions (with final states A_{g-} and A_{g+}) are red-shifted relative to the monomeric absorption peak $S_0 \rightarrow S_1$ and may be allowed in 2PA transitions due to the same parity of these two states as defined by selection rules. We suggest that these calculated $A_g \rightarrow A_g$ transitions correspond to the experimental 2PA bands with peak positions at 2.05 eV (excitation at 1210 nm) and 1.86 eV (excitation at 1330 nm), labeled as (2) and (3) in Figure 3. The next four transitions shown in Table 1 are derived from 2PA transitions, $S_0 \rightarrow S_2$, in each monomer. They correspond to two allowed $A_g \rightarrow B_u$ (also with different oscillator strengths) and two forbidden $A_g \rightarrow A_g$ transitions. In our 2PA measurements, we can observe only one band at longer wavelengths with a final state of A_{g-} symmetry. The $A_g \rightarrow A_g$ transition (with a final state of A_{g+} symmetry) corresponding to the shorter wavelength cannot be observed due to the close proximity of the 1PA edge.

On the basis of the quantum chemical calculations, we conclude that the dimer's three transitions $S_0 \rightarrow S_1$, $S_0 \rightarrow S_3$, and $S_0 \rightarrow S_6$ are 2PA allowed given that the parities of the states are the same. They are labeled as (3), (2), and (1) in Figure 3, respectively. Note that the 2PA transition $S_0 \rightarrow S_6$ in the dimer is the combination of $(HOMO\text{-}1)_+ \rightarrow LUMO_+$ and $(HOMO\text{-}1)_- \rightarrow LUMO_-$, similar to the strongest 2PA transition ($S_0 \rightarrow S_2$) in the monomer corresponding to HOMO−1→LUMO. Therefore, the 2PA transition in the dimer (labeled as (1) in Figure 3) adopts the same configuration, but slightly red-shifts in spectral position with respect to the monomer 2PA transition (labeled as (1′) in Figure 3). The two other 2PA transitions of the dimer (labeled as (2) and (3) in Figure 3) are different and correspond to the combination of $HOMO_- \rightarrow LUMO_-$ and $HOMO_+ \rightarrow LUMO_+$. These 2PA bands are strongly red-shifted with respect to the HOMO→LUMO transition in the monomer. Thus, while the π-stacking dimers are similar to H-aggregates, they lead to a red shift in 2PA transition, which is opposite to the well-known blue shift in linear spectra upon formation of H-aggregates.[32]

In conclusion, we report the 2PA spectrum of a D-π-A cyanine-like dye G19 single crystal with a strong polarization-dependent anisotropy in both linear and nonlinear optical properties. The maximum 2PA coefficient, 52 ± 9 cm/GW, measured at 2.76 eV (excitation at 900 nm) with the polarization angle 45° with respect to one crystal facet, is ~2.5× larger than that of a bulk inorganic semiconductor, CdTe, having a similar absorption edge, although the averaged 2PA cross section in the crystal is 20× less than that extrapolated from its toluene solution due to strong

dx.doi.org/10.1021/jz300222h | J. Phys. Chem. Lett. 2012, 3, 1222−1228

intermolecular interactions. X-ray analysis shows that molecules in the single crystal form dimers arranged by two dye molecules aligned in an antiparallel manner. According to quantum chemical calculations, this dimerization leads to a splitting of the energy levels into in- and out- of phase combinations with opposite parities, and thus results in the appearance of new red-shifted 2PA bands as compared to the monomer form in toluene.

EXPERIMENTAL SECTION

The synthesis of G19 is described in ref 33. A solution growth technique by self-nucleation of a slightly subsaturated hot solution of acetonitrile was utilized to obtain single crystals. This subsaturated solution was prepared with a temperature just below the solvent boiling points (82 °C). It was then sealed and placed in a hot water bath inside a vacuum Dewar to allow slow cooling to room temperature in order to promote single crystal formation. A standard microscope (Olympus BX51) captured the image of the single crystal with a digital camera, and dimension scales were calibrated against a standard micrometer (see Figure 1b). The same microscope was also used to measure the reflection spectra of the single crystal.

The linear transmittance of the G19 crystal under unpolarized illumination was measured by an Ocean Optics spectrometer USB4000-UV−vis with a tungsten−halogen white light source Oriel 66184. The polarization angle-dependent linear transmittance spectra were measured by placing an uncoated calcite polarizer in front of the sample. The spot size of the light beam was restricted to ∼300−500 μm in order to under-fill the sample. X-ray diffraction analysis at ∼100 K was performed on a Bruker Smart ApexII X-ray diffractometer. Details of the X-ray experiment and the obtained crystallographic data are presented in CIF format in the Supporting Information.

The ND-2PA spectrum of the G19 crystal was obtained using a conventional femtosecond excite-probe technique[34] employing an optical parametric generator/amplifier (OPA/OPG, model TOPAS-800 pumped by Clark-MXR CPA-2010 at a 1 kHz repetition rate) as the tunable excitation source (300 nm to 2.6 μm). A small portion of the fundamental laser pulse was focused into a 1 cm water cell to generate a white-light-continuum probe. The wavelength of the probe beam was selected by interference filters of sufficient bandwidth to transmit ∼140 fs pulses verified by ND-2PA excite-probe experiments. The spot size of the probe beam was set to be ∼6× smaller than that of the excitation beam with an angle of ∼5−10° between the beams to ensure the probe experienced a homogeneous excitation irradiance. The polarization angle was determined by rotating a half-wave plate in front of the sample. Both excitation and probe beams were kept copolarized, i.e., they were linearly polarized at the same angle θ. To measure the polarization angle dependence of the linear transmittance of the crystal, the excitation beam was blocked, and the transmitted probe beam at 1.30 eV (950 nm) was measured.

The D-2PA spectrum of the crystal was measured with the same femtosecond laser as previously stated by an open-aperture Z-scan.[35] Bulk semiconductors of CdSe and CdTe were used as reference samples to characterize and verify the setup and accuracy, respectively.[24] Special care was taken to make sure that the laser beam was exciting the same spot on the crystal for all Z-scan measurements. The Z-scan curves showed a background due to sample inhomogeneities and/or surface irregularities that were subtracted using the technique described in detail in ref 35.

ASSOCIATED CONTENT

Supporting Information

The reflection spectra, excite-probe for ND-2PA, and Zscan trace for D-2PA of the G19 crystal. This material is available free of charge via the Internet http://pubs.acs.org

AUTHOR INFORMATION

Corresponding Author

*E-mail: ewvs@creol.ucf.edu.

Notes

The authors declare no competing financial interest.

ACKNOWLEDGMENTS

This work is supported in part by the Air Force Office of Scientific Research (AFOSR) FA9550-10-1-0558 and the DARPA ZOE Program W31R4Q-09-1-0012. X-ray studies and quantum chemical calculations were supported by the NSF via the PREM program, Grant 0934212 and CHE 0832622 (P.T., T.V.T., I.H.N., and A.E.M.). The CPU time on the Stockes supercomputer system at UCF IST is gratefully acknowledged. We thank Dr. Pieter Kik and students Mr. Chatdanai Lumdee and Mr. Seyfollah Toroghi for use of their optical microscope and reflection setup.

REFERENCES

(1) Cumpston, B. H.; Ananthavel, S. P.; Barlow, S.; Dyer, D. L.; Ehrlich, J. E.; Erskine, L. L.; Heikal, A. A.; Kuebler, S. M.; Lee, I. Y. S.; McCord-Maughon, D.; et al. Two-Photon Polymerization Initiators for Three-Dimensional Optical Data Storage and Microfabrication. *Nature* **1999**, *398*, 51−54.

(2) Belfield, K. D.; Ren, X.; Van Stryland, E. W.; Hagan, D. J.; Dubikovsky, V.; Miesak, E. J. Near-IR Two-Photon Photoinitiated Polymerization Using a Fluorone/Amine Initiating System. *J. Am. Chem. Soc.* **2000**, *122*, 1217−1218.

(3) Parthenopoulos, D. A.; Rentzepis, P. M. Three-Dimensional Optical Storage Memory. *Science* **1989**, *245*, 843−845.

(4) Hagan, D. J. In *Handbook of Optics*; 3rd ed.; Bass, M., Ed.; McGraw Hill: New York, 2010; Vol. *IV*, p 13.11.

(5) Zipfel, W. R.; Williams, R. M.; Webb, W. W. Nonlinear Magic: Multiphoton Microscopy in the Biosciences. *Nat. Biotechnol.* **2003**, *21*, 1369−1377.

(6) Zhao, L.; Xu, J. J.; Zhang, G.; Bu, X.; Shionoya, M. Frequency-Upconverted Organic Crystal. *Opt. Lett.* **1999**, *24*, 1793−1795.

(7) Bauer, C.; Schnabel, B.; Kley, E. B.; Scherf, U.; Giessen, H.; Mahrt, R. F. Two-Photon Pumped Lasing from a Two-Dimensional Photonic Bandgap Structure with Polymeric Gain Material. *Adv. Mater.* **2002**, *14*, 673−676.

(8) Fang, H.-H.; Xu, B.; Chen, Q.-D.; Ding, R.; Chen, F.-P.; Yang, J.; Wang, R.; Tian, W.-J.; Feng, J.; Wang, H.-Y.; et al. Two-Photon Absorption and Spectral-Narrowed Light Source. *IEEE J. Quantum. Elect.* **2010**, *46*, 1775−1781.

(9) Said, A. A.; Sheik-Bahae, M.; Hagan, D. J.; Wei, T. H.; Wang, J.; Young, J.; Van Stryland, E. W. Determination of Bound-Electronic and Free-Carrier Nonlinearities in ZnSe, GaAs, CdTe, and ZnTe. *J. Opt. Soc. Am. B* **1992**, *9*, 405−414.

(10) Nootz, G.; Padilha, L. A.; Olszak, P. D.; Webster, S.; Hagan, D. J.; Stryland, E. W. V.; Levina, L.; Sukhovatkin, V.; Brzozowski, L.; Sargent, E. H. Role of Symmetry Breaking on the Optical Transitions in Lead-Salt Quantum Dots. *Nano Lett.* **2010**, *10*, 3577−3582.

(11) Marder, S. R. Organic Nonlinear Optical Materials: Where We Have Been and Where We Are Going. *Chem. Commun.* **2006**, 131−134.

(12) Van Stryland, E. W.; Hagan, D. J.; Przhonska, O. V.; Marder, S. R.; Webster, S.; Padilha, L. A. Nonlinear Absorption Spectroscopy of Organic Dyes. *Nonlinear Opt., Quantum Opt.* **2010**, *40*, 95−113.
(13) Padilha, L. A.; Webster, S.; Hu, H.; Przhonska, O. V.; Hagan, D. J.; Van Stryland, E. W.; Bondar, M. V.; Davydenko, I. G.; Slominsky, Y. L.; Kachkovski, A. D. Excited State Absorption and Decay Kinetics of Near IR Polymethine Dyes. *Chem. Phys.* **2008**, *352*, 97−105.
(14) Fu, J.; Padilha, L. A.; Hagan, D. J.; Van Stryland, E. W.; Przhonska, O. V.; Bondar, M. V.; Slominsky, Y. L.; Kachkovski, A. D. Experimental and Theoretical Approaches to Understanding Two-Photon Absorption Spectra in Polymethine and Squaraine Molecules. *J. Opt. Soc. Am. B* **2007**, *24*, 67−76.
(15) Padilha, L. A.; Webster, S.; Przhonska, O. V.; Hu, H.; Peceli, D.; Rosch, J. L.; Bondar, M. V.; Gerasov, A. O.; Kovtun, Y. P.; Shandura, M. P.; et al. Nonlinear Absorption in a Series of Donor-π-Acceptor Cyanines with Different Conjugation Lengths. *J. Mater. Chem.* **2009**, *19*, 7503−7513.
(16) Przhonska, O. V.; Webster, S.; Padilha, L. A.; Hu, H.; Kachkovski, A. D.; Hagan, D. J.; Van Stryland, E. W. In *Advanced Fluorescence Reporters in Chemistry and Biology I: Fundamentals and Molecular Design*, Springer Series in Fluorescence; Demchenko, A. P., Ed.; Springer-Verlag: Berlin Heidelberg, 2010.
(17) Chung, S.-J.; Zheng, S.; Odani, T.; Beverina, L.; Fu, J.; Padilha, L. A.; Biesso, A.; Hales, J. M.; Zhan, X.; Schmidt, K.; et al. Extended Squaraine Dyes with Large Two-Photon Absorption Cross-Sections. *J. Am. Chem. Soc.* **2006**, *128*, 14444−14445.
(18) Polyakov, S.; Yoshino, F.; Liu, M.; Stegeman, G. Nonlinear Refraction and Multiphoton Absorption in Polydiacetylenes from 1200 to 2200 nm. *Phys. Rev. B* **2004**, *69*, 115421.
(19) Fang, H.-H.; Chen, Q.-D.; Yang, J.; Xia, H.; Ma, Y.-G.; Wang, H.-Y.; Sun, H.-B. Two-Photon Excited Highly Polarized and Directional Upconversion Emission from Slab Organic Crystals. *Opt. Lett.* **2010**, *35*, 441−443.
(20) Zheng, M.-L.; Chen, W.-Q.; Fujita, K.; Duan, X.-M.; Kawata, S. Dendrimer Adjusted Nanocrystals of DAST: Organic Crystal with Enhanced Nonlinear Optical Properties. *Nanoscale* **2010**, *2*, 913−916.
(21) Komorowska, K.; Brasselet, S.; Dutier, G.; Ledoux, I.; Zyss, J.; Poulsen, L.; Jazdzyk, M.; Egelhaaf, H. J.; Gierschner, J.; Hanack, M. Nanometric Scale Investigation of the Nonlinear Efficiency of Perhydrotriphenylene Inclusion Compounds. *Chem. Phys.* **2005**, *318*, 12−20.
(22) Zheng, M.-L.; Fujita, K.; Chen, W.-Q.; Duan, X.-M.; Kawata, S. Two-Photon Excited Fluorescence and Second-Harmonic Generation of the DAST Organic Nanocrystals. *J. Phys. Chem. C* **2011**, *115*, 8988−8993.
(23) Fang, H.-H.; Yang, J.; Ding, R.; Chen, Q.-D.; Wang, L.; Xia, H.; Feng, J.; Ma, Y.-G.; Sun, H.-B. Polarization Dependent Two-Photon Properties in an Organic Crystal. *Appl. Phys. Lett.* **2010**, *97*, 101101.
(24) Sheik-Bahae, M.; Hutchings, D. C.; Hagan, D. J.; Van Stryland, E. W. Dispersion of Bound Electron Nonlinear Refraction in Solids. *IEEE J. Quantum Electron.* **1991**, *27*, 1296−1309.
(25) Klocek, P. *Handbook of Infrared Optical Materials*; Marcel Dekker Inc.: New York, 1991.
(26) Monson, P. R.; McClain, W. M. Polarization Dependence of the Two-Photon Absorption of Tumbling Molecules with Application to Liquid 1-Chloronaphthalene and Benzene. *J. Chem. Phys.* **1970**, *53*, 29−37.
(27) Patel, P. D.; Masunov, A. E. Theoretical Study of Photochromic Compounds. 1. Bond Length Alternation and Absorption Spectra for the Open and Closed Forms of 29 Diarylethene Derivatives. *J. Phys. Chem. A* **2009**, *113*, 8409−8414.
(28) Toro, C.; Thibert, A.; De Boni, L.; Masunov, A. E.; Hernandez, F. E. Fluorescence Emission of Disperse Red 1 in Solution at Room Temperature. *J. Phys. Chem. B* **2008**, *112*, 929−937.
(29) Cardenas-Jiron, G. I.; Masunov, A.; Dannenberg, J. J. Molecular Orbital Study of Crystalline P-Benzoquinone. *J. Phys. Chem. A* **1999**, *103*, 7042−7046.
(30) Masunov, A. E.; Grishchenko, S. I.; Zorkii, P. M. Effect of Specific Intermolecular Interactions on Crystalline-Structure - Uracyl Derivatives and Analogs. *Zh. Fiz. Khim.* **1993**, *67*, 221−239.
(31) Frisch, M. J.; Trucks, G. W.; Schlegel, H. B.; Scuseria, G. E.; Robb, M. A.; Cheeseman, J. R.; Montgomery, J., J. A.; Vreven, T.; Kudin, K. N.; Burant, J. C.et al. *Gaussian 2003*; Gaussian, Inc: Wallingford, CT, 2004.
(32) Passier, R.; Ritchie, J. P.; Toro, C.; Diaz, C.; Masunov, A. E.; Belfield, K. D.; Hernandez, F. E. Thermally Controlled Preferential Molecular Aggregation State in a Thiacarbocyanine Dye. *J. Chem. Phys.* **2010**, *133*, 134508.
(33) Gerasov, A. O.; Shandura, M. P.; Kovtun, Y. P. Series of Polymethine Dyes Derived from 2,2-Difluoro-1,3,2-(2H)-dioxaborine of 3-Acetyl-7-diethylamino-4-hydroxycoumarin. *Dyes Pigm.* **2008**, *77*, 598−607.
(34) Negres, R. A.; Hales, J. M.; Kobyakov, A.; Hagan, D. J.; Van Stryland, E. W. Experiment and Analysis of Two-Photon Absorption Spectroscopy Using a White-Light Continuum Probe. *IEEE J. Quantum Electron.* **2002**, *38*, 1205−1216.
(35) Sheik-Bahae, M.; Said, A. A.; Wei, T.-H.; Hagan, D. J.; Van Stryland, E. W. Sensitive Measurement of Optical Nonlinearities Using a Single Beam. *IEEE J. Quantum Electron.* **1990**, *26*, 760−769.